Summer 8-7-2021

Development of a Microfluidic Viscoelastic Hemostatic Assay for Real-Timeviscosity Measurements of Blood

Shay Kent

DEVELOPMENT OF A MICROFLUIDIC VISCOELASTIC HEMOSTATIC ASSAY FOR REAL-TIME VISCOSITY MEASUREMENTS OF BLOOD

A Thesis

Submitted to Duquesne University

Duquesne University

In partial fulfillment of the requirements for

the degree of Master of Science

By

Shay Kent

August 2021

DEVELOPMENT OF A MICROFLUIDIC VISCOELASTIC HEMOSTATIC ASSAY

FOR REAL-TIME VISCOSITY MEASUREMENTS OF BLOOD

By

Shay Kent

Approved July 7, 2021

Dr. Melikhan Tanyeri
Assistant Professor
(Committee Chair)

Dr. Kimberly Williams
Associate Professor
(Committee Member/Reader)

Dr. Bin Yang
Assistant Professor
(Committee Member/Reader)

Dr. John Viator, Professor
Chair, Department of
Engineering

Dr. Fevzi Akinci, Professor
Dean, Rangos School of Health
Sciences

ABSTRACT

DEVELOPMENT OF A MICROFLUIDIC VISCOELASTIC HEMOSTATIC ASSAY FOR REAL-TIME VISCOSITY MEASUREMENTS OF BLOOD

By

Shay Kent

August 2021

Thesis supervised by Dr. Melikhan Tanyeri

Blood coagulation disorders are malfunctions in the body's ability to control blood clotting. It can result in either insufficient clotting causing an increased risk of bleeding or excessive clotting obstructing blood flow. The rapid and accurate diagnosis of coagulopathies is an important, unmet need in the clinical setting. Rapidly identifying the source of bleeding, either acquired or inherited, is critical to reduce the risk of major blood loss and deliver personalized hemostatic therapies. Viscoelastic hemostatic assays, or VHAs, deliver an effective solution to the diagnosis of coagulopathies by evaluating global hemostatic function using whole blood rather than plasma. VHAs are functional blood tests that monitor all phases of coagulation by measuring the viscoelastic properties of blood during clot formation and degradation to help determine the root cause of bleeding. Presently, the two major commercialized VHA techniques are the thromboelastometry (TEM) and the thromboelastography (TEG). These two instruments, however, have a high

acquisition cost, bulky benchtop size, and are mostly limited to use in surgical procedures. Here, we aim to develop a microfluidic viscoelastic hemostatic assay (μVHA) to facilitate point-of-care hemostatic tests based on digital microfluidics where whole blood samples are partitioned into nanoliter sized emulsion droplets. These devices have been fabricated using soft lithography techniques and are capable of determining viscoelastic properties of coagulating blood as a function of time. We employ digital microfluidics where blood samples are split into nanoliter sized droplets within a microchannel under constant pressure, and viscoelastic properties of blood are deduced from droplet properties such as droplet length and inter-droplet distance. The length of the droplets is correlated with aqueous phase viscosity at high ratios of aqueous-to-oil inlet pressure. Here, we demonstrate a proof-of-concept blood coagulation analysis device that can potentially deduce viscoelastic properties of whole blood under low shear conditions, thereby providing information about global hemostatic function from the beginning of clot formation through clot retractions and fibrinolysis. These portable and low cost μVHAs would ultimately reduce the footprint and overall cost, broaden potential applications beyond emergency and surgical procedures and enable adoption by military medics for field diagnosis of combat trauma patients.

ACKNOWLEDGEMENT

I would like to acknowledge Dr. Tanyeri for all his help and advice while working on this project. I would also like to acknowledge the members of the Tanyeri Lab, Alex Evans, Selvin Hernandez, Shawn Bliss, Timmy Pecoraro and Adriana Del Pino Herrera for their help on this project.

TABLE OF CONTENTS

LIST OF FIGURES

Page

LIST OF ABBREVIATIONS

VHA – Viscoelastic Hemostatic Assay

TEG – Thromboelastography

TEM – Thromboelastometry

CCT – Conventional Coagulation Test

Hb – Hemoglobin

PT – Prothrombin Time

aPTT – activated Partial Thromboplastin Time

INR – International Normalized Ratio

μVHA – microfluidic viscoelastic hemostatic assay

R – reaction time

K – kinetics

Alpha – slope between reaction time and kinetics

MA – maximum amplitude

CL – clot lysis

CT – clotting time

CFT – clot formation time

MCF – maximal clot firmness

LY – lysis

Q_S/Q_C – sample to carrier fluid flow rate ratio

η_{sample}– sample viscosity

m – coefficient determined empirically

b – coefficient determined empirically

L_c – minimal droplet length that the droplets converge to

L_d – droplet length

cP – centipoise

ASAP – actuated surface-attached posts

PDMS – polydimethylsiloxane

Chapter I

Introduction

1.1 Introduction

The rapid and accurate diagnosis and immediate initiation of treatment of coagulopathies are an important, unmet need in the clinical setting to prevent unnecessary mortality and morbidity [1]. In order to reduce the risk of major blood loss and deliver personalized hemostatic therapies, it is critical to rapidly identify the source of bleeding, either acquired or inherited. In the field of emergency care, diagnosis of coagulopathies requires quick diagnostic tools [2]. For effective diagnosis and treatment of chronic diseases such as cardiovascular diseases, certain biomarkers, such as blood viscosity, need to be routinely monitored, therefore diagnostic tools that require small sample volumes that can be carried out at the point-of-care show great potential [3].

1.2 Microfluidic Technology

Microfluidic technology, or lab-on-a-chip devices, manipulates miniscule amounts of fluids [4]. Microfluidic technology has emerged rapidly in various fields ranging from medical diagnosis to chemical synthesis [5]. At the microscale, gravitational forces are greatly reduced and other forces such as capillary forces, surface tensions, and viscous forces become more dominant [6]. The efficient transport of reactants within a miniaturized device allows for faster diagnosis, resulting in a decrease in cost, on-site testing and

diagnosis [5]. Droplet-based microfluidic systems generate a large number of isolated volumes via emulsions of two or more immiscible phases allowing each individual droplet to perform a different reaction from another droplet, therefore enabling parallel processing and multiplexing of reactions without significantly increasing device size or complexity [7]. A novel aspect of droplet microfluidics is the ability to produce uniform droplets at a high throughput without material exchange between droplets [7]. On-site testing using small sample sizes such as those from droplets would potentially allow for obtaining continuous blood viscosity data from patients, thereby improving diagnosis and treatment accuracy [5]. Microfluidic devices are revolutionizing the field of medical diagnosis by providing patients and healthcare providers with point-of-care diagnostic tools [8]. The integration and automation of the lab-on-a-chip systems remain as major challenges to their wide-spread adoption in many biological fields [5, 8].

1.3 Blood Coagulation

There are three pathways that make up the blood coagulation pathway: the intrinsic, extrinsic, and common pathway (Figure 1.3.1). Each of these pathways is governed by

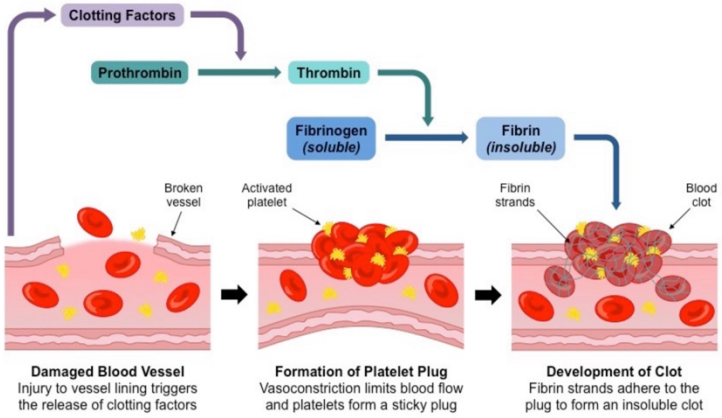

Figure 1.3.1 Clot formation: A diagram of clot formation.

biochemical interactions and coagulation factors [9]. A bleeding disorder is typically associated with the deficiency of one of the coagulation factors [10]. For instance, when tissue damage occurs, blood begins to clot to plug up the damaged tissue. First, clotting factors are released in response to an injury, followed by vasoconstriction of the blood vessels to limit blood flow and platelets form a plug. Then fibrin strands attach to the plug and form a clot. Conventional tests do not provide a global assessment of hemostatic function and biochemical processes that play a role during the clot formation process [11, 12]. Viscoelastic hemostatic assays provide better insights into the coagulation cascade as it is performed with whole blood.

1.4 Conventional Coagulation Tests

Bleeding disorders are routinely diagnosed by a panel of conventional coagulation tests, or CCTs [2, 11, 12]. CCTs are widely used in clinical settings to assess blood clotting function and can be extremely useful for identifying and characterizing bleeding disorders of secondary hemostasis [13]. The typical tests in a CCT panel include Hemoglobin concentration (Hb), hemocrit, platelet count, fibrinogen level, prothrombin time (PT), activated partial thromboplastin time (aPTT), international normalized ratio (INR), and D-dimer. In these tests, blood samples are treated in vitro with an array of activation factors to measure the coagulation time [13, 14]. For example, prothrombin time is a plasma-based assay that evaluates the extrinsic and common pathways (specifically factors VII, X, V, II, and fibrinogen) where calcium and thromboplastin, a tissue factor and platelet phospholipids, are added to blood plasma to initiate the fibrin clot formation [9, 15]. The typical time to fibrin gel formation for PT is approximately 10-14 seconds [16].

Prolongation of the PT usually implies a defective extrinsic and/or common pathways [17]. An aPTT test evaluates the intrinsic and common pathway where calcium, platelet phospholipids, and an activator (silica, celite, kaolin, or ellagic acid) are added to blood plasma to determine the clotting time in the absence of tissue factors [18]. The typical time to fibrin gel formation for aPTT is typically 20-50 seconds and prolongation of the aPTT indicates defective intrinsic and/or common pathways.

The panel of CCTs, however, have numerous limitations as well [19]. For instance, CCTs do not measure the balance of the hemostatic components through all phases, from clot initiation through clot lysis and only provide end point measurements [2, 12, 20, 21]. They also do not account for the balance between coagulation and fibrinolysis, and therefore, are not sufficient to explain the pathways leading to hemostasis in vivo [20]. CCTs are limited in detecting the type of hypercoagulation and the shortening of PT/aPTT time is not a consistent predictor of hypercoagulability [12, 14, 22]. These tests cannot identify the root cause for certain bleeding disorders, especially induced coagulopathies or trauma-induced coagulopathies [22-25]. CCTs in general, and in vitro plasma-based tests such as PT and aPTT in particular, do not account for important interactions between molecular and cellular components (e.g. platelets, fibroblasts and clotting factors) in platelet activation and thrombin generation, as they are based on the cascade model of coagulation [26, 27]. Further, PT/aPTT tests do not assess overall strength and stability of clots as they are measured at the initiation of fibrin polymerization [12, 20, 21]. PT/aPTT do not detect hyperfibrinolysis or platelet dysfunction and are not prolonged until fibrinogen falls to very low levels [28]. CCTs are not point-of-care assays and long processing times can lead to treatment delays which is associated with mortality and

morbidity, especially under time-constrained circumstances such as trauma and surgery [2, 23, 29, 30]. Therefore, when CCTs fall short in providing sufficient diagnostic information, Viscoelastic Hemostatic Assays are performed to gain more insight into global hemostatic function.

1.5 Viscoelastic Hemostatic Assays

Viscoelastic hemostatic assays, or VHAs, deliver an effective solution to the diagnostic testing of coagulopathies by evaluating global hemostatic function using whole blood rather than plasma [2, 12, 14, 21, 31]. VHAs are functional blood tests that monitor all phases of coagulation by measuring the viscoelastic properties of blood during clot formation and degradation to help determine the root cause of bleeding [12]. The current commercialized VHA methods are the Thromboelastometry (TEM) and the Thromboelastography (TEG). These two instruments, however, have a high acquisition cost, bulky benchtop size, and are mostly limited to use in surgical procedures [32]. Here, I demonstrate a proof-of-concept device which can potentially be developed into microfluidic viscoelastic hemostatic assay (μVHA) to facilitate point-of-care hemostatic tests using a method based on digital microfluidics where whole blood samples are partitioned into nanoliter sized emulsion droplets. These portable and low cost μVHAs would reduce the footprint and overall cost of analytical systems, broaden potential applications beyond emergency and surgical procedures and would enable field/combat medics providing frontline trauma and medical care to deployed personnel [2, 4, 8, 14, 21].

VHAs provide a point-of-care global and functional assessment of hemostasis by revealing contributions and interactions of all hemostatic components during clot

formation [12, 20]. Viscoelastic properties of the blood clot are evaluated starting at initiation of coagulation through amplification and propagation of the clot to fibrinolysis [12, 32]. VHAs help determine the root cause of bleeding and evaluate how fibrinogen forms fibrin [33]. Fibrin is an insoluble protein that is responsible for forming blood clots. It forms a fibrous mesh that will impede the flow of blood. VHAs enable diagnosis of both inherited and acquired bleeding disorders, including post-traumatic coagulopathies and mechanisms underlying traumatic hemorrhage, are often used as a diagnostic tool to guide patient-specific transfusion therapy [29, 34-36]. VHAs have several advantages over the typical panel of conventional coagulation tests, or CCTs, including providing an overview of global hemostatic function. First, they provide information on all phases of hemostasis, including initial fibrin formation, fibrin-platelet plug construction, and clot lysis [2, 12]. Second, VHAs are also capable of diagnosing hypo-coagulable conditions that are not evident with CCTs. They facilitate rapid diagnosis of coagulopathies and reduces overall transfusion requirements [20]. VHAs have been proven superior in predicting and diagnosing coagulopathies, guiding transfusion therapy, and found clinical applications in cardiac surgery, liver transplantation and obstetric hemorrhage [22, 35-38]. In cardiac surgery, where the risk of surgical bleeding or induced coagulopathy is higher, VHAs can help identify patients needing peri operative (mid-operation) or postoperative (after operation) transfusion therapy [27, 36, 37]. Transfusion therapy guided by VHAs reduces the frequency of blood product transfusions (red blood cells and platelets) and major bleeding following cardiac surgery [34, 39]. The advancements in VHAs will allow for point-of-care testing which yields quicker results and enables wider adoption of the method in emergency and operating rooms [12, 40]. Specifically, VHAs lead to cost-effective

practices for trauma and cardiac surgery patients in comparison to typical CCTs [39, 41]. Closely mimicking the major physiological processes of hemostasis in vitro helps providing insights into the root cause of bleeding disorders where plasma-based conventional coagulation tests (PT, aPTT, INR) have limitations in detecting impaired hemostasis [24, 27, 41].

Even though VHAs provide several advantages over the panel of CCTs that are usually used to diagnose coagulation disorders, they still have some limitations. Due to their bulky instrumentation size and high price tag, their implementation is currently limited to patients with trauma or undergoing surgical procedures [23]. The commercial VHA instruments are mainly used in operating rooms and emergency care units [40]. Their use in medical procedures is also limited to a few procedures including transfusion therapy, liver transplant, trauma, and cardiac surgery [23, 37, 38]. To increase the versatility and wide-spread adoption of VHAs in the biomedical field, improvements in blood sample handling, full automation of the assay protocols, simultaneous testing with multiple activators, integrated analysis software and enhancing robustness of the device are needed [2].

1.6 Thromboelastography and Thromboelastometry

Two of the most common VHAs on the market today are the Thromboelastography (TEG) and the Thromboelastometry (TEM). The TEG was first described in 1948 by Hartert who measured the viscoelastic changes of whole blood during coagulation under

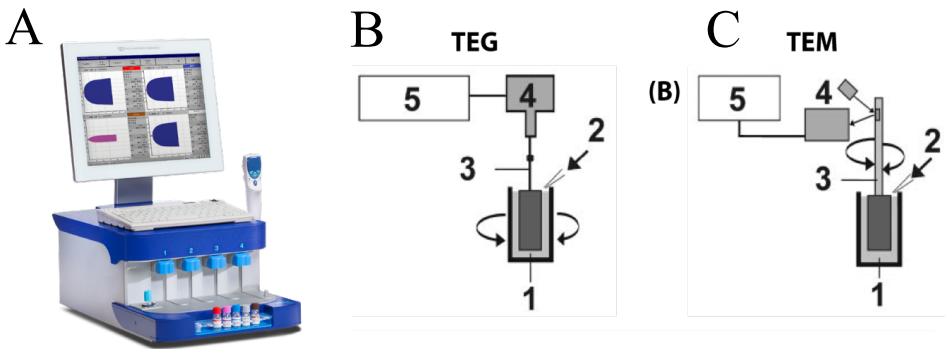

Figure 1.6.1 Major commercialized VHA systems: (A) An image of a commercial thromboelastometry (TEM) system. The schematic of (B) the TEG system and (C) the TEM system. Component 1 represents the cup, 2 represents the blood sample, 3 represents the pin, 4 represents the transducer (optical/electrochemical) and 5 represents the data processing unit (Adapted from [20]).

low shear conditions [42]. He developed a graphical representation of the rate of fibrin polymerization and the overall clot strength, although the technique was not adopted for clinical use until the 1980s [3, 32]. The TEM was developed in 1995 as an enhancement for hemostasis testing in whole blood, providing differential diagnostic information [3, 32]. Both processes rely on a transducer that measures clot firmness as a function of time where 300uL whole blood is placed into a cylindrical cup at 37 degrees Celsius [3, 12, 32]. A suspended pin is inserted into the cup, and the viscoelastic properties of blood clots are deduced by monitoring changes in the rotation of the pin (Figure 1.6.1). The pin is not in direct contact with the cup and the blood sample provides the physical link between the cup and the pin (Figure 1.6.1b-c). Coagulation activators are then added to the sample and coagulation is triggered by oscillating either the cup (TEG) or the pin (TEM) back and forth around the vertical axis [3, 12, 32]. The torque acting on the pin due to rotation is minimal at the beginning of the process. As the blood coagulates, the blood sample starts forming a clot between the cup and the pin which generates a torque proportional to clot

firmness which is transmitted to the pin. The pin is connected to a detector system which measures torque applied to the pin. In the TEG, the detector system is a torsion wire and in the case of TEM, it is an optical detector [2, 3, 12, 32]. The strength of the formed clot is measured with an electromechanical (TEG) or an optomechanical (TEM) transducer during the coagulation process. The TEG and TEM curves produced from the process show clot firmness as a function of time.

The transducer data collected from the coagulation process are converted into TEG/TEM curves displaying clot firmness as a function of time (Figure 1.6.2a). From these curves, we can deduce the parameters representing characteristics of coagulation and the lysis process [2, 3, 12, 32]. The key parameters for a TEG curve include reaction time (R), kinetics (K), maximum amplitude (MA), clot lysis (CL), and the slope of K and α (alpha). The key parameters for a TEM curve include clotting time (CT), clot formation time (CFT), maximal clot firmness (MCF), lysis (LY), and the slope of the tangent at 2mm amplitude (α). Reaction time, or clotting time, represents the time of latency, the time from the start of the test to the initial fibrin formation and is typically between 15 and 23 minutes [2, 3, 12]. Kinetics, or clot formation time represents the time to achieve a certain level of clot strength and is typically between 5 and 10 minutes. The maximum amplitude, or maximal clot firmness, is a function of the dynamic properties of fibrinogen and represents the ultimate strength of the clot before it starts to degrade. The alpha angle (α) measures the fibrin build-up and cross-linking speed, assessing the clot formation speed. The curves are divided into parts that reveal different successive stages of the hemostatic process, from initiation of coagulation to fibrinolysis. The typical TEG/TEM for a healthy patient shows a coagulation trace in the shape of a horizontal champagne flute. Anomalies seen in the

TEG/TEM curves are used to diagnose inherited or acquired bleeding disorder (Figure 1.6.2b). In the presence of a coagulopathy (a coagulation disorder), the shape of the coagulation trace is modified, hinting at the root cause of coagulopathy [2, 3, 12]. The shape of the TEG/TEM curves can be analyzed to associate them with specific coagulopathies and then develop patient-specific therapies. For instance, hypercoagulation is diagnosed when reaction time (R) or clotting time (CT) is shortened; kinetics (K) or clot formation time (CFT) is also shortened; max amplitude (MA) or max clot firmness (MCF) is increased. Another example includes hemophilia where coagulation trace features show longer reaction time (R) or clotting time (CT), longer kinetics (K) or clot formation time (CFT), and smaller max amplitude (MA) or maximum clot firmness (MCF). Using the process of creating the TEG/TEM curves and deriving the key parameters from those

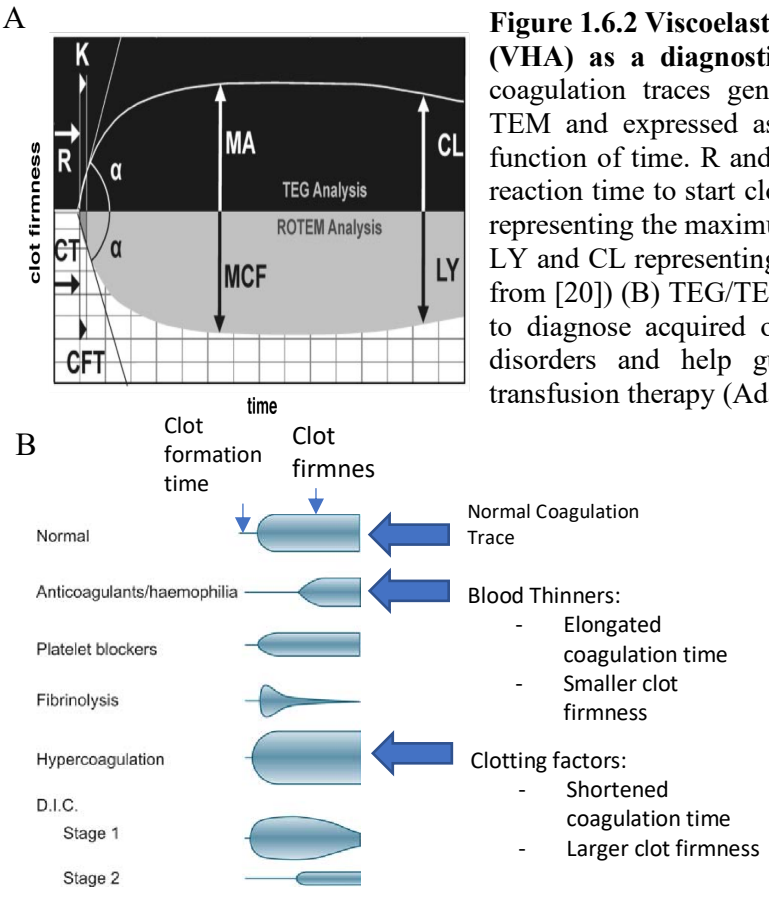

Figure 1.6.2 Viscoelastic Hemostatic Assay (VHA) as a diagnostic tool: (A) Typical coagulation traces generated by TEG and TEM and expressed as clot firmness as a function of time. R and CT representing the reaction time to start clotting. MA and MCF representing the maximum clot firmness, and LY and CL representing clot lysis. (Adapted from [20]) (B) TEG/TEM traces can be used to diagnose acquired or inherited bleeding disorders and help guide patient-specific transfusion therapy (Adapted from [3]).

curves, it is possible to use anomalies in the curves to diagnose inherited or acquired bleeding disorders [23].

Even though the TEG and TEM are valuable tools for diagnosing inherited or acquired bleeding disorders, they do have some limitations. Both systems have a high acquisition cost. The TEG that is commercialized by Hemoscope Corporation, which is currently a subsidiary of Haemonetics, and its two-channel TEG 5000 system costs over $18K. The ROTEM delta, a four-channel rotational TEM system developed by TEM International GmbH (now part of Werfen) costs nearly $28K. The cost of running a "basic test" is about $10 and the platelet function test costs about $90. Finally, their bulky benchtop size limit widespread use of commercial TEG/TEM systems, mainly restricting their use in surgical procedures [1, 2].

1.7 Microfluidic Viscoelastic Hemostatic Assays (μVHA)

In this work, we propose to develop a microfluidic viscoelastic hemostatic assay (μVHA), a more accessible and low-cost diagnostic tool to facilitate point-of-care hemostatic tests. Our method is based on digital microfluidics where whole blood samples are partitioned into nanoliter sized emulsion droplets [1, 2, 43, 44]. These portable and low cost μVHAs would reduce the footprint and overall cost of analytical systems, broaden potential applications beyond emergency and surgical procedures. Our approach would enable development of field deployable platforms that can be utilized by military medics in trauma care immediately after injury to determine course of action and increase the effectiveness of treatment. Utilizing a digital microfluidic approach and implementing an optofluidic method to generate coagulation traces, it will transform the existing VHA

methods based on electromechanical or optomechanical transduction by mitigating its shortcomings and potentially extending its applications in biomedical fields [20, 39]. The μVHA is based on an established microfluidic technology, digital microfluidics, which involves generation and manipulation of nanoliter sized droplets within microchannels [7, 45]. Blood samples are partitioned into droplets using a flow-focusing geometry by squeezing the sample stream by two orthogonal immiscible carrier fluid streams at a microfluidic junction where the stream is broken into monodisperse nanoliter sized droplets [7, 46]. During the emulsification process, droplet size and inter-droplet distance is dictated by the device and flow parameters such as device geometry (channel height, widths, and lengths), absolute and relative flow rates of sample fluid (e.g. blood) and immiscible carrier fluid, and the relative viscosities of the sample and carrier fluids [1, 43, 44, 47]. Droplet size and inter-droplet distance during droplet breakup process can be used to monitor changes in sample fluid viscosity [43]. For a given device geometry and sample-to-carrier fluid flow rate ratio (Q_S/Q_C), the droplet length decreases as the viscosity of the sample fluid increases [43]. As the coagulation process proceeds, the viscosity of the blood increases which leads to a reduction in droplet length [44]. In this manner, using the correlation between viscosity and droplet length, the viscosity of the blood can be actively monitored as a function of time during the coagulation process. Dynamic blood viscosity measurements during coagulation process allows for generation of clot firmness curves that are obtained through conventional VHA methods including TEG and TEM. Our goal is to develop a proof-of-concept, portable microfluidic VHA (μVHA) to generate coagulation traces throughout the coagulation process, similar to those from the TEG/TEM, for rapid and accurate diagnosis of bleeding disorders.

1.8 Novelty of our Approach

The novelty of our approach is based on an innovative engineering tool, digital microfluidics, to enhance the status quo in coagulation monitoring by providing an enabling new technology for rapid diagnosis of bleeding disorders. The device will be an automated, droplet-based method for real-time monitoring of whole blood coagulation in vitro. Viscoelastic properties of whole blood during clot formation and degradation will be monitored using an optofluidic method. A microfluidic approach enables reduction of the sample size by a factor of 3, down to 100uL, and allow for parallel testing of various versions of VHAs using a single blood sample [2]. Reduction of the sample size and parallel testing potentially opens new applications of coagulation monitoring in point-of-care testing [26, 38, 48]. For instance, reducing the sample size below 100μL could extend the application of VHAs to pediatric procedures [49]. The microfluidic system will shrink the overall size of the coagulation monitoring instrument, therefore reducing the cost and increasing portability [43, 50]. Mixing of the coagulation initiators will be automated which will minimize human errors encountered in TEG/TEM-based assays, improving reliability and robustness of viscoelastic coagulation assays [44, 51]. This method will also have the ability to measure non-Newtonian fluids and will be readily applicable to measure viscoelastic properties of other limited-volume biological samples such as cerebrospinal fluid, pleural fluid, and amniotic fluid for diagnostic purposes [52].

In μVHA, coagulation process and clot stiffness are monitored by quantitatively analyzing the droplet breakup process; and coagulation traces similar to the TEG/TEM systems are generated The slope of the linear relationship between the sample and the quantity given by $1/(L_d - L_c)$ determines the sensitivity and the range of viscosity

measurements. This slope can be adjusted by the device and flow parameters such as channel dimensions, carrier fluid viscosity, absolute and relative flow rates of blood and immiscible carrier fluid [43, 44]. As the ratio of the sample flow rate to the carrier fluid flow rate (Q_S/Q_C) increases, the sensitivity of measuring the viscosity measurements increases [43]. The range and sensitivity of the viscosity measurements can be tuned towards a specific application by adjusting the device geometry and flow parameters [43].

Our method relies on generating coagulation traces similar to the TEG/TEM systems by analyzing the droplet size and inter-droplet distance during the droplet breakup process. Using the coagulation traces, it is possible to derive fundamental parameters characterizing the coagulation process such as clot formation time, maximal clot firmness, and clot lysis. This requires extensive analysis of how microfluidic device geometry and flow parameters affect the generation of coagulation traces. Initially, the focus will be on testing samples from healthy individuals to demonstrate the applicability of the method to monitor coagulation using normal blood samples. To test the validity of our approach, the μVHA devices will be tested using samples from healthy individuals that are spiked with inhibitors and thrombin to mimic and hypercoagulable state with excessive blood clotting. The results will be compared against those from the TEG and TEG systems to illustrate the feasibility of this device towards the diagnosis of bleeding disorders.

Our approach has the potential to widen the adoption of VHAs by clinicians in procedures where blood loss or bleeding disorders have to be evaluated in the diagnostic and therapeutic decision-making process. The small size of the device will help reduce the footprint and overall cost the system, therefore broadening the potential applications of VHAs in medical practices beyond emergency and surgical procedures. The proposed

method will reduce the sample size three times, enable automatic fluid handling, increase the multiplexing capability by allowing more assays to run simultaneously in parallel, and substantially shrink the footprint of the instrumentation to enable portable and/or field-deployable devices [53].

Chapter II

Microfluidic Viscoelastic Hemostatic Assay for Real-Time Viscosity Measurements

2.1 Introduction

Viscosity of chemical and biological fluids is an important materials property. In medical diagnostics, changes in physical and chemical properties of biofluids can be correlated to a number of diseases. Laborious procedures, high testing cost and larger sample sizes are typical limitations associated with continuous viscosity measurements and, therefore, characterization of viscosity is often limited to end-point measurements [50]. Miniaturized viscometers can be developed using microfabrication and microfluidic technology, and the incorporation of droplet microfluidics can further reduce sample size from microliters to nanoliters [43, 47, 50, 51]. Here, we report a continuous droplet-based viscometer to measure viscosity of aqueous fluids based on the size and length of emulsified droplets generated under constant pressure.

2.2 Device Design

We tested several designs for our microfluidic viscometer and the final version comprised of one oil inlet, one aqueous solution inlet and one outlet (Figure 2.2.1).

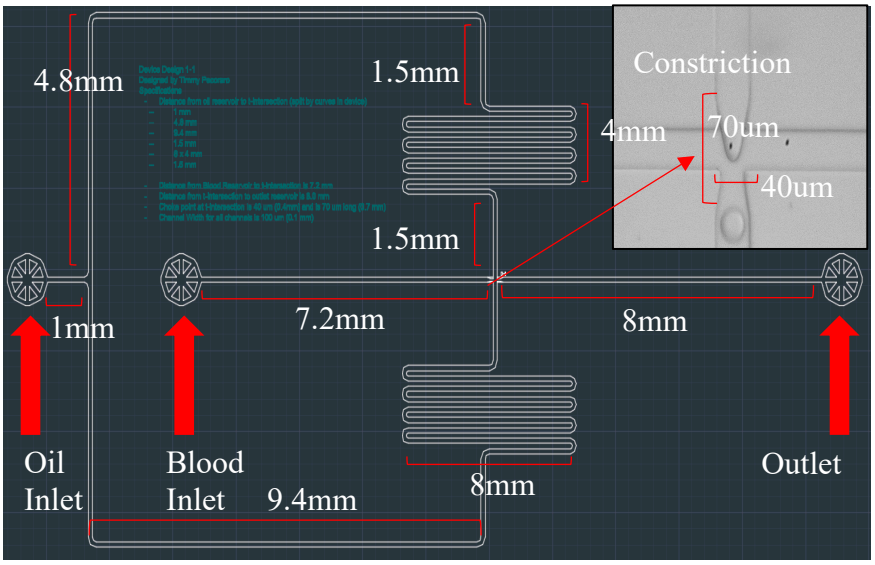

Figure 2.2.1 Microfluidic viscometer device design: We designed a microfluidic device consisting of one oil inlet, one aqueous solution inlet and one common outlet channel. The length of the oil inlet, aqueous inlet, and outlet channels were 50.2mm, 7.2mm and 8mm, respectively. Droplets are generated at a junction where the oil and aqueous inlets meet. The channel width and height across the device was 100 and 50 µm, respectively. The aqueous inlet and the outlet channel contained a 40µm wide and 70µm long constriction at the junction.

Mask Design:

The device designs were created using AutoCAD software. The device geometry was inspired by Li et. al. [43, 44]. The device consists of a droplet generator using a flow focusing geometry where a microchannel carrying the aqueous sample solution meets a perpendicular channel at a microfluidic junction. At this junction, the aqueous sample is split into droplets by two opposing streams of immiscible oil. The oil inlet was split into two channels which has a total length of 50.2 mm up to the microfluidic junction where it

meets with the sample/aqueous inlet. The length of the aqueous/sample channel was 7.2 mm. Droplets generated at the microfluidic junction were carried down an 8 mm long outlet channel. All channel widths were 100 µm. At the microfluidic junction, the aqueous/sample channel and the outlet channel had a 40 µm wide constriction, which facilitated droplet generation. Channel height was approximately 50 µm which was determined by the thickness of the SU-8 during photolithography process. The dimensions of this device are shown in Figure 2.2.1.

2.3 Device Fabrication

The device is fabricated by conventional photolithography and soft lithography techniques [54] (Figure 2.3.1).

Cleanroom Procedures:

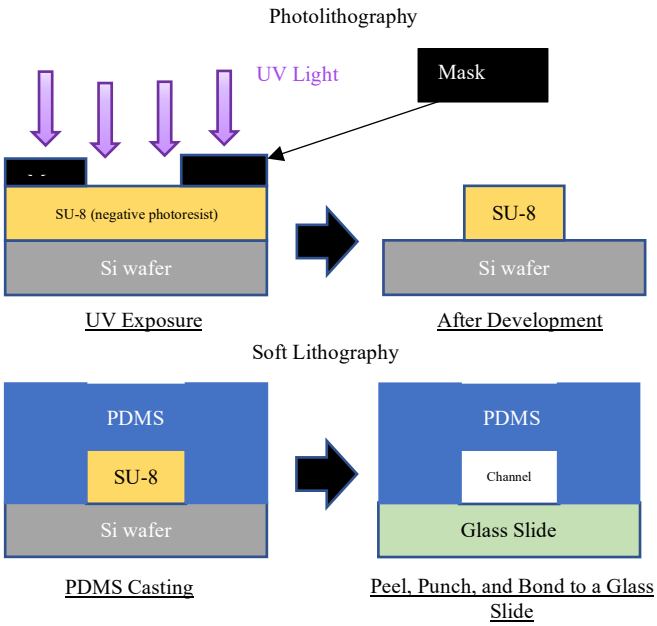

Figure 2.3.1 Device fabrication: Fabrication process of microfluidic devices with photolithography and soft lithography.

Gowning:

A special gown including a coverall, shoe covers, boots, hair net, hood and gloves must be worn when fabricating the devices in the cleanroom to minimize dust and contamination.

SU-8 Coating:

Silicon wafers were cleaned using acetone and isopropyl

alcohol and dried off with compressed dry air. The wafers were then placed on a hot plate (Torrey Pines EchoTherm HS40A) at 65 degrees Celsius to remove any surface water. After cleaning, the wafer was carefully placed on the spin coater (Laurell, WS-650Mz-23NPPB), centering it to the chuck. Prior to spin coating step, the wafer was secured to the chuck by turning on the vacuum. A small amount of SU-8 2050 was dispensed onto the wafer such that the photoresist covered about 2/3 of the wafer. Any bubbles in the photoresist were carefully removed using a plastic disposable pipet. We then run the following program to spin coat the wafer with the photoresist:

1.) Spin at 500 rpm for 5-10 seconds with acceleration of 100 rpm/second.

2.) Spin at 2000 rpm for 30 seconds with acceleration of 300 rpm/second.

This procedure typically yields 50 μm thick device features on the SU-8 mold. During spin-coating, a build-up of photoresist, called edge bead, can occur on the edge of the substrate. A swab dipped in acetone can be used to wipe the edge of the wafer to minimize its impact on photomask contact during the lithography step. We then performed a soft bake step, 3 minutes at 65°C and 9 minutes at 95°C, as suggested by the manufacturer.

Exposure:

To obtain vertical sidewalls with SU-8 2050, a long pass filter was used to eliminate UV radiation below 350 nm. The wafer was placed under the UV flood exposure unit (350W Model LS-150-3 NUV Exposure System, Bachur Associates) and the desired mask was placed on the wafer, a quartz slab was then placed on top of the wafer to bring the mask and the wafer into conformal contact. The wafer was then exposed to UV light for approximately 11 seconds.

Post Exposure Bake:

The wafer was baked for 1-2 minutes at 65°C, then for 6-7 minutes at 95°C. After 1 minute of baking at 95°C, an image of the mask was visible in the photoresist. If no visible latent image is seen during or after PEB, the exposure, post-baking (or both) was insufficient.

Development:

We immersed the wafer to the solvent-based developer, PGMEA, for 7 minutes. The development times are approximate, since actual dissolution rates can vary widely as a function of agitation. While immersed, the wafer was agitated to fully remove any uncrosslinked SU-8. If successful, no white streaks should appear on the wafer. The wafer and SU-8 features should look clean and transparent.

Rinse and Dry:

The mold was then rinsed with isopropyl alcohol 3-4 times and dried with compressed dry air. The mold was then stored within a petri dish in the cleanroom.

Hard Baking (optional):

SU-8 has good mechanical properties, therefore hard bakes are normally not required. When cracks were observed in the device features, we hard-baked the wafer by gradually ramping the temperature up to 150°C, baking at this temperature for 5 minutes, then cooling it down to room temperature.

<u>PDMS Chip Fabrication:</u>

PDMS Preparation:

To prepare the wafer for replica molding, the wafer was silanized by adding a few drops of silane into a petri dish, then incubating under vacuum for 15-30 minutes. PDMS was

prepared by mixing the base and the cross-linker component at a 10:1 (by mass) ratio. The two were mixed together in a plastic cup and degassed using a vacuum desiccator. The PDMS mixture was then poured onto the wafer in the petri dish. The wafer was placed into an oven at 75 degrees Celsius for a minimum of two hours.

Preparing the final device:

After taking the PDMS wafer out of the oven, it was left to cool down to room temperature. Then, using a scalpel, the PDMS layer was carefully cut out of the petri dish. Holes were punched into the PDMS to form the inlet and outlet ports for each device.

Cutting:

Using a razor blade, the PDMS slab was cut into sections that will fit onto a glass slide. Depending on the size of the devices, there could be many devices on a PDMS slab that can fit on one slide. We typically obtained two devices per 1x3" microscope slide.

Bonding:

The PDMS slabs were cleaned by adhesive tape to remove any dust particles and PDMS fragments from punching inlet and outlet ports. The PDMS slabs and clean glass slides were placed into the chamber of a plasma cleaner (Harrick Plasma PDC-001) and exposed to oxygen plasma at a power of 30W for approximately 20 seconds. The PDMS slabs containing microfluidic device features should face-up on the glass tray. After plasma activation, the PDMS and glass slide were brought into conformal contact to obtain a complete device. The bonded devices were put into a petri dish and baked at 75 degrees Celsius overnight.

Silanization:

Prior to each experiment, we silanized our microfluidic devices using Aquapel (PPG Industries). Briefly, aquapel solution was transferred into a 1mL glass, gas-tight syringe, and the solution was introduced into the oil inlet port. The device was carefully filled with the Aquapel solution. 8-10 devices were treated at one time, allowing each device to be exposed to Aquapel solution for approximately 30-60 seconds. Next, using an empty syringe, air was pushed through each device to expel the Aquapel solution and dry the device. A second syringe with ethanol was used to wash the devices and remove any residual Aquapel. Subsequently, the empty syringe was used again to flow air through the devices to remove ethanol. The devices were then baked at 75 degrees Celsius for at least 20 minutes.

2.4 Experimental Setup:

The experimental setup consisted of a microfluidic device, an inverted microscope, a CCD camera, two electronic pressure regulators and a computer (Figure 2.4.1). The microfluidic chip was mounted onto the microscope (Nikon TS100) stage with a 4x objective lens, and images and videos were captured with a CCD camera (Basler acA800-510um). The glass slide was secured to the stage using tape to keep the device in focus during the experiment. 2 mL of the aqueous solution was transferred into a glass vial with a screw cap with precision-fit silicone and PTFE septum providing a leak-proof seal. The oil solution (Light mineral oil, Fisher Scientific) was also transferred into a similar container. Polymer tubing (Saint-Gobain Tygon Tubing, ND-100-80, .020" ID x .060" OD) with a metal tubing (New England Small Tube, NE-1310-03) at each end was used to

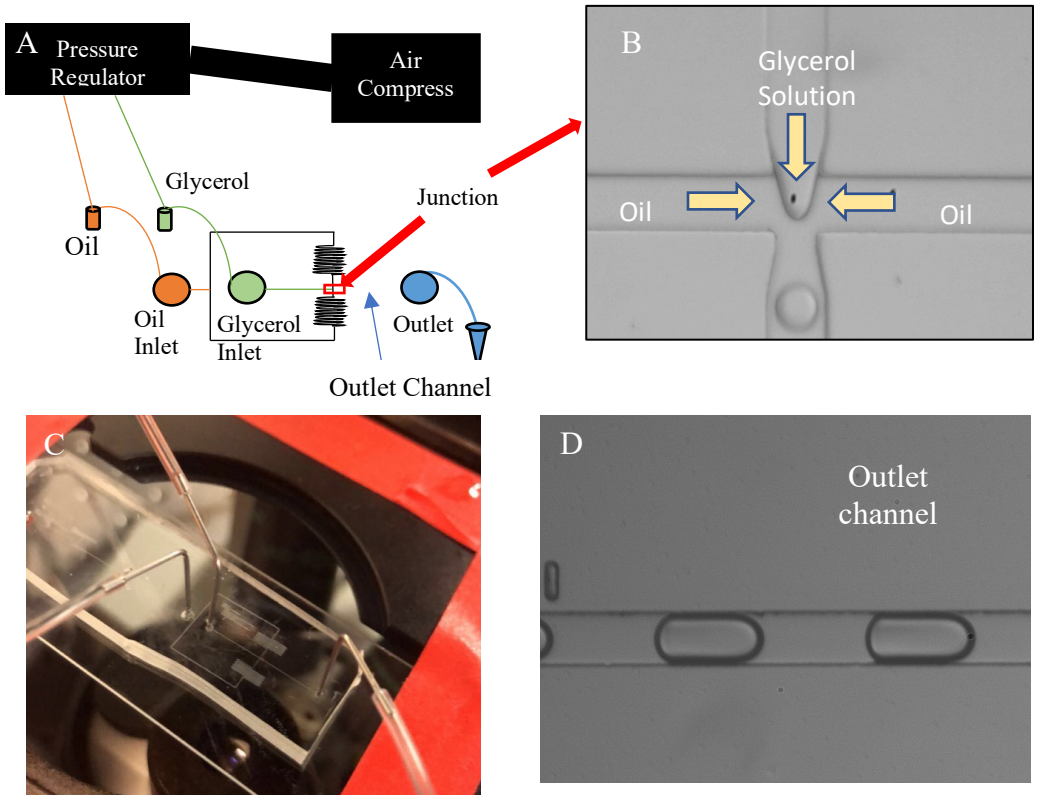

Figure 2.4.1 Experimental setup for microfluidic viscometer: (A) Schematic of the experimental setup (B) Micrograph of droplet generation at the microfluidic junction (C) an image of the microfluidic device mounted on the microscope. (D) Image of droplets produced by the device in the outlet channel.

introduce fluids for each inlet. One end of the tubing was inserted through the septum of the vial and the other end, bent at a ninety-degree angle, was inserted into the device. Each inlet and outlet tubing is inserted into the device in a similar manner. Compressed dry air was fed into an electronic pressure regulator (ProportionAir, MPV1MBHEEZP30PSGAXL) to control air pressure through each inlet (Figure 2.4.1). Compressed dry air through the pressure regulator is connected to the vials containing the aqueous sample and the oil. The electronic pressure regulator was controlled by a custom LabVIEW code, where the magnitude of air pressure for both solutions was adjusted within 0-30 psi. The same device was used for conducting viscosity measurements for different

solutions. Between each measurement, the device was flushed by compressed dry air. Droplet images were captured along the outlet microchannel at a position just below the microfluidic junction. Droplet images were analyzed and droplet parameters including droplet length were extracted using ImageJ and MATLAB.

2.5 Solution Preparation

Aqueous Solutions:

Blood viscosity ranges within 0-60 cP at medium shear rates (80-100 sec^{-1}) for healthy individuals [55]. We prepared aqueous glycerol solutions ranging from 1 to 60 cP to mimic various stages of blood coagulation and used these solutions as the aqueous phase for the droplet generation. The solutions were created by mixing water and glycerol as given below, and the viscosity values were confirmed by a commercial rotational viscometer (Brookfield LVDV-II+CP). We prepared the glycerol solutions using a table reporting viscosity of glycerol and its aqueous solutions at various % weight (Table 2.5.1). We confirmed viscosity of each sample solution using a cone and plate viscometer (Figure 2.5.1). Our results are in good agreement with the tabulated viscosity values for glycerol solutions. We further measured the viscosity of a human blood

Glycerol (% weight)	Viscosity (cP) @ 20ºC
0	1.005
20	1.76
50	6
60	10.8
70	22.5
75	35.5
80	60.1

Table 2.5.1: Viscosity and % weight of aqueous glycerol solutions mimicking various stages of blood coagulation used in the experiments.

sample with the rotational viscometer and found out that the blood viscosity was approximately 9.75cP.

Oil Solution:

For the oil phase, we used light mineral oil (CAS 8042-47-5, Fisher Scientific). To facilitate droplet generation, 10% Silube (T308-16, Siltech Corporation) was added to the oil phase as surfactant.

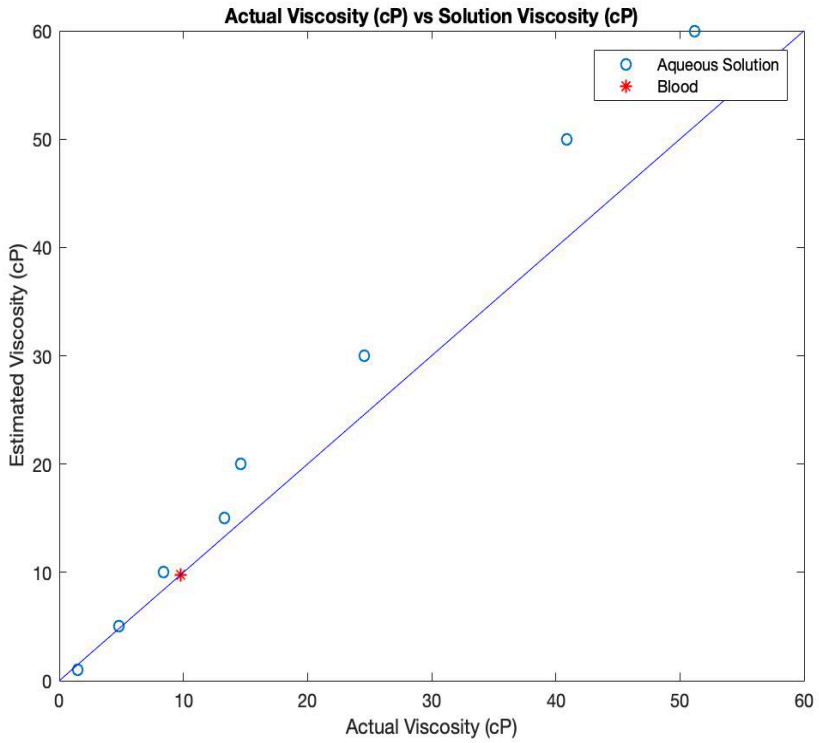

Figure 2.5.1 Viscosity measurements of glycerol solutions using a commercial cone-and-plate viscometer: The plot displays expected viscosity values for glycerol solutions shown in Table 2.5.1 versus the viscosity measurements performed with a rotational viscometer. The red star in the figure represents viscosity measurement for a human blood sample.

2.6 Measurements

Using the LabVIEW program, the air pressure was regulated to flow oil and aqueous solution through the device (Figure 2.6.1). Droplets were formed at the junction where the aqueous phase was pinched by the oil phase. Flow rates through the inlets are

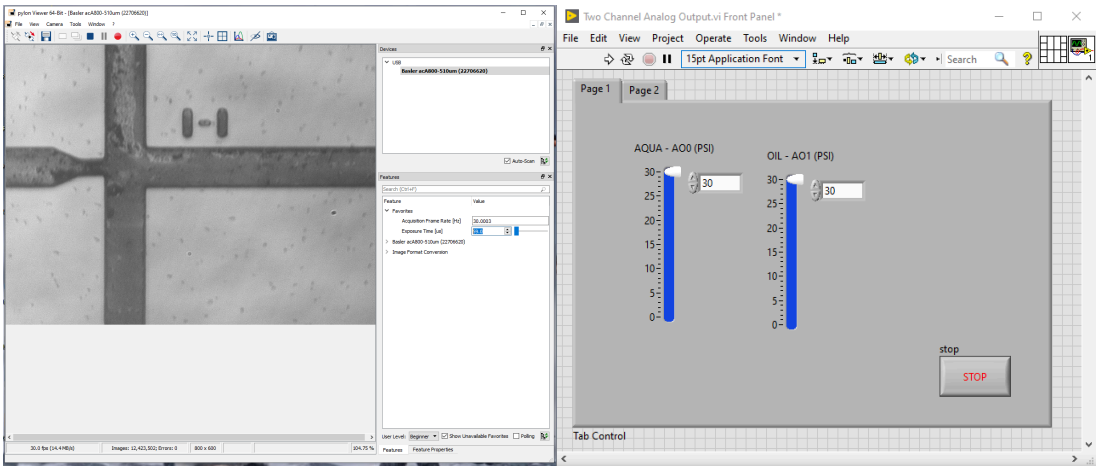

Figure 2.6.1 Experimental setup control: (A) Image of the microfluidic junction as observed during experiments and (B) the LabVIEW interface used to control flow with the pressure regulator.

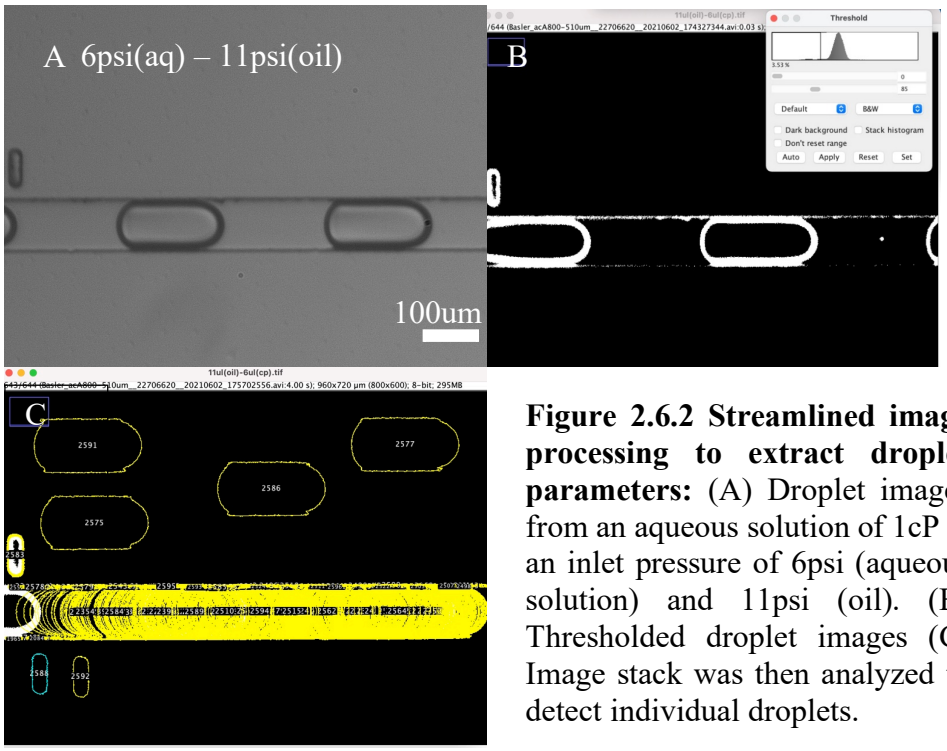

Figure 2.6.2 Streamlined image processing to extract droplet parameters: (A) Droplet images from an aqueous solution of 1cP at an inlet pressure of 6psi (aqueous solution) and 11psi (oil). (B) Thresholded droplet images (C) Image stack was then analyzed to detect individual droplets.

controlled by individually adjusting the pressure applied to each inlet. For efficient droplet generation, the oil phase should have a higher flow rate compared to the aqueous phase. Using a CCD camera, we acquired videos of droplet formation for two minutes at the beginning and end of an experimental run. In between videos, images were captured every second for ten minutes. Using ImageJ, images were converted into a stack and processed to determine the average length of the droplets (Figure 2.6.2). Briefly, droplet images were first converted into stacks. The 8-bit images were then thresholded for binary conversion. Then, we ran particle detection algorithms in ImageJ to detect each droplet and extract its key parameters including droplet length.

2.7 Results

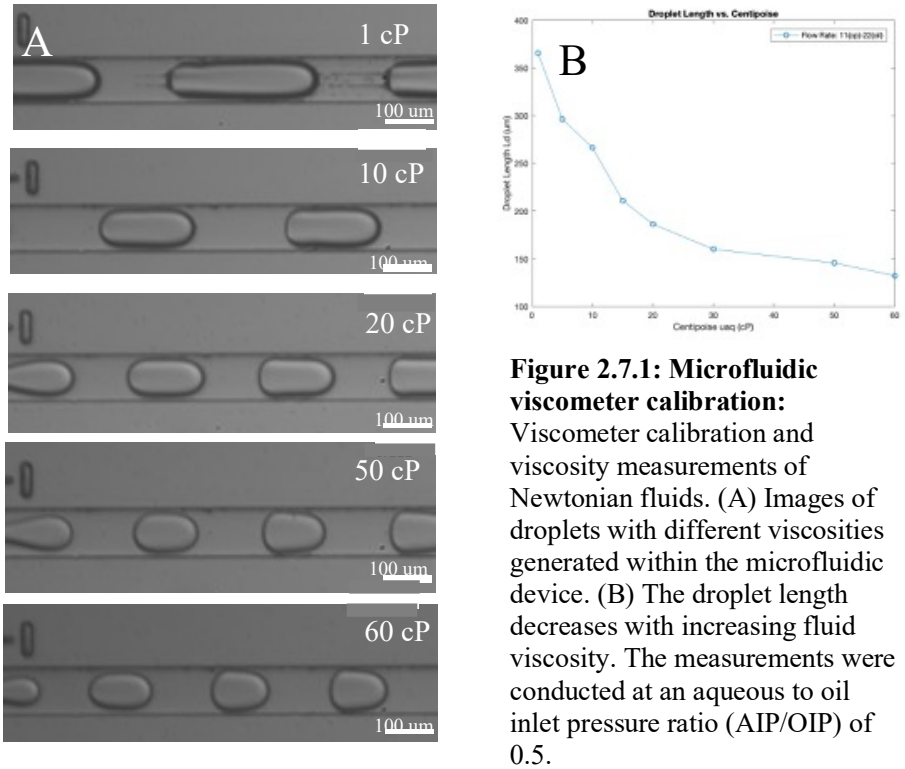

Figure 2.7.1: Microfluidic viscometer calibration: Viscometer calibration and viscosity measurements of Newtonian fluids. (A) Images of droplets with different viscosities generated within the microfluidic device. (B) The droplet length decreases with increasing fluid viscosity. The measurements were conducted at an aqueous to oil inlet pressure ratio (AIP/OIP) of 0.5.

The droplet-based viscometer uses pressure driven flow of an aqueous glycerol solution and mineral oil for droplet generation at a microfluidic junction and a

downstream channel for droplet measurement. Oil and glycerol solutions are introduced to the microchannels using various inlet pressures and the droplets are then dispensed into a centrifuge tube via the outlet tubing. At the junction, the aqueous phase is pinched by the two opposing oil streams and droplets form in the downstream outlet channel. The size of the droplets depends on the flow rate of the aqueous and the oil phase, the higher the ratio of oil to aqueous solution, the smaller the droplets become. Droplet size is also directly related to the viscosity of the aqueous solution. At a fixed pressure ratio, the length of the droplet is inversely related to the viscosity of the aqueous solution, as the viscosity increases from 1cP to 60cP, the droplet length decreases. A calibration curve was constructed to show a linear relationship between η_{aq} and $1/(L_D - L_C)$ (or an

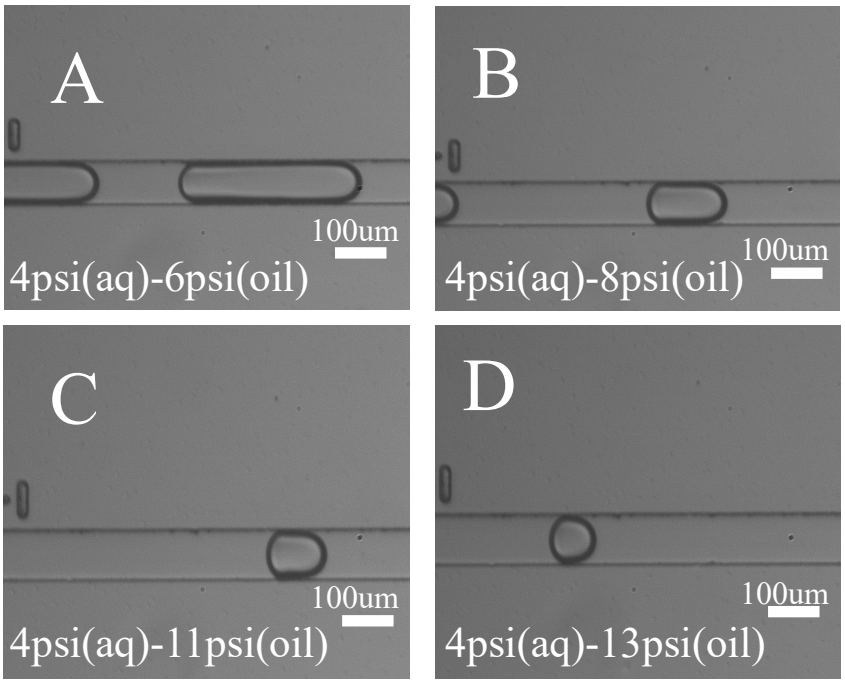

Figure 2.7.2: Effect of AIP/OIP on droplet size: Images of droplets generated using 1cP aqueous solution and light mineral oil. The aqueous inlet pressure (AIP) is kept at 4psi, while the oil inlet pressure (OIP) is changed from (A) 6psi to (B) 8psi to (C) 11psi to (D)13psi. As OIP is increased, where AIP/OIP decreases, the droplet length decreases from (A) 417.98µm to (B) 195.64µm to (C) 145.33µm to (D) 119.99 µm.

inverse relationship between the droplet length and the aqueous phase viscosity) that can be used to calculate sample viscosities (Figure 2.7.1).

To generate droplets, the device needs to be operated such that the ratio of the aqueous inlet pressure to oil inlet pressure, denoted by AIP/OIP, is within a certain range. We focused on finding this optimal ratio range for each aqueous sample viscosity and then determining which AIP/OIP ratio would yield consistent droplets across viscosity values within 1-60cP (Figure 2.7.2). When the AIP/OIP is below the optimal range, the oil pressure is too high and causes the aqueous solution to retract back up the sample channel and no droplets can be formed. When the AIP/OIP is above the optimal range, the aqueous sample flow rate is too high, and it forms a stream, rather than generating droplets, that co-flows with the oil phase as the oil flow is insufficient to pinch the aqueous phase. Within

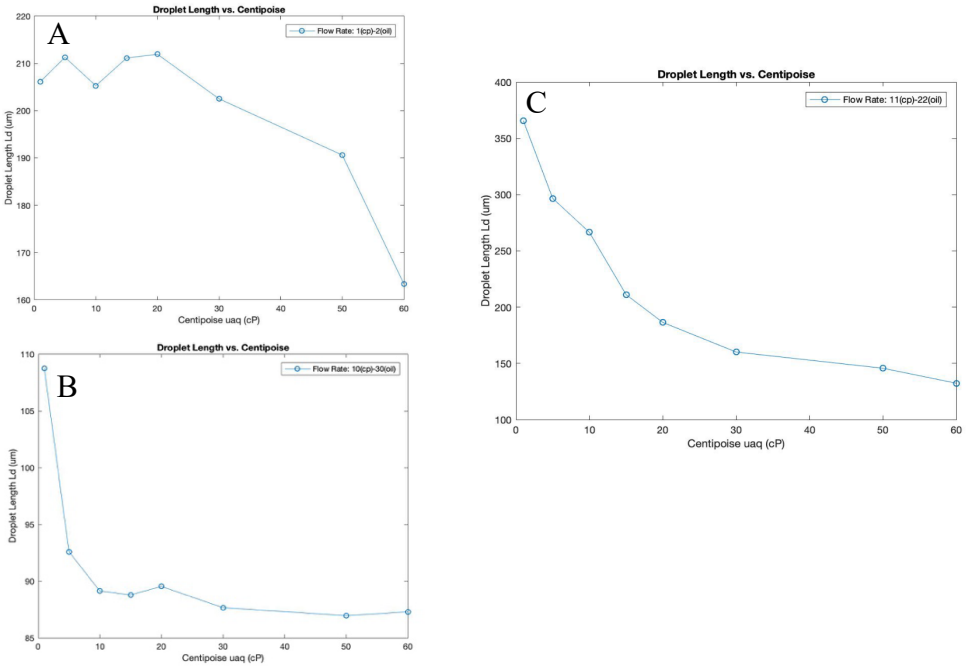

Figure 2.7.3 Droplet length at various aqueous phase viscosities and AIP/OIP ratios: Droplet length versus aqueous phase viscosity demonstrating an inverse relationship. As the viscosity increases, the droplet length will decrease at a given flow rate. (A) 1psi(aq)-2psi(oil), (B) 10psi(aq)-30psi(oil), (C) 11psi(aq)-22psi(oil).

the optimal range of AIP/OIP, the droplet size increases with increasing AIP/OIP (Figure 2.7.2). The optimal value of AIP/OIP ratio should be the highest AIP/OIP that still generates a steady train of droplets without distortion. The sensitivity of the device to measure changes in viscosity increases with the AIP/OIP ratio, as can be seen in the viscosity versus droplet length curve (Figure 2.7.3). As the flow rate increases (while keeping the aqueous to oil inlet pressure ratio constant), the slope of the viscosity versus droplet length plot also increases, indicating an increase in sensitivity (Figure 2.7.3). Optimal results were obtained at high flow rates. For instance, setting the aqueous inlet pressure to 11psi and the oil inlet pressure to 22psi (AIP/OIP = 0.5) provided a wide dynamic range with high sensitivity for viscosity measurements (Fig. 2.7.3c).

Chapter III

Whole Blood Analysis

3.1 Introduction

Abnormalities in blood clot formation is a major cause of morbidity and mortality worldwide. In emergency medicine, uncontrolled bleeding is a major cause of death that can be prevented [30, 40]. Coagulopathy, acidosis, and hypothermia are often referred to as the "trauma triad of death" [23, 30]. It is reported that about one-fourth of trauma patients suffer from coagulopathy [56]. Coagulopathy is also a major complication of sepsis and leads to rapid death with over 1 million cases of sepsis per year resulting in 250,000 deaths [27, 57]. With early diagnosis and early intervention and treatment, deaths due to coagulopathy can be prevented.

Non-Newtonian fluids, such as blood, are viscoelastic and their viscosities depend on shear rate. To characterize the viscosity profile of a non-Newtonian fluids, there are two types of viscometers, the cone-and-plate viscometers and capillary viscometers [50]. Rotational viscometers, such as the cone-and-plate viscometer, measure viscosity based on a velocity-driven flow field while capillary viscometers use pressure-driven flow to measure viscosity [50]. An advantage of the capillary viscometers is their ability to simulate real flow in tubular channels, such as blood vessels.

Droplet-based viscometers demonstrate advantages over existing microfluidic viscometers such as lower sample volume, higher potential for automation, continuous

operation capabilities and device reusability [43, 44, 47]. However, the droplet-based viscometer has not yet been proven to measure viscosities for all types of fluids, such as non-Newtonian fluids and highly viscous fluids. In this research, we use previously developed droplet-based viscometer methods and apply them to measure viscosities of non-Newtonian fluids.

3.2 Results

Using our microfluidic viscometer, we performed viscosity measurements with human whole blood samples (Figure 3.2.1). Specifically, we introduced human whole blood samples with anticoagulants through the aqueous inlet and generated micron-sized droplets in mineral oil (Figure 3.2.1, top panels). We observed a similar trend with the droplet breakup process. We compared the length of the droplets from the blood sample to those from the aqueous glycerol solutions. We determined that droplet sizes for the blood

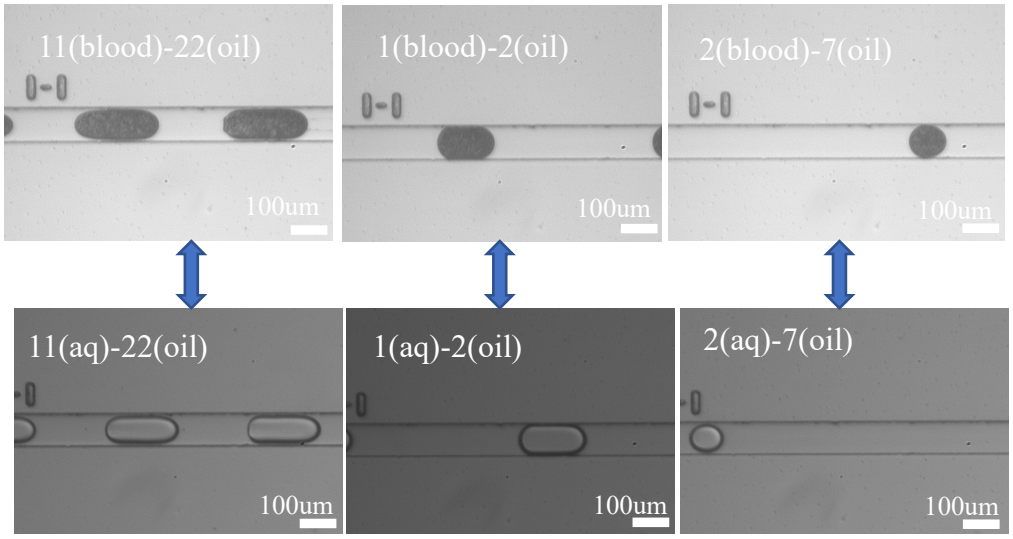

Figure 3.2.1: Droplet-based viscosity measurements of human whole blood samples: Droplet images comparing blood sample (top panels) and corresponding aqueous glycerol solutions (bottom panel). We observed that the average droplet length from blood samples were similar to those from 10cP glycerol solution.

sample closely matched the 10cP aqueous glycerol solution. Therefore, we concluded that the viscosity of the blood sample is approximately 10cP at the shear rates (~20 s^{-1}). To further confirm this, we overlayed the data point obtained from the blood sample to the calibration plot obtained using aqueous glycerol solutions (Figure 3.2.2). We observed that the viscosity measurement for the blood sample lies on the droplet length vs. aqueous viscosity plot at the same aqueous and oil inlet pressures (and the same corresponding AIP/OIP). Viscosity of human whole blood samples range between 2-6 cP prior to coagulation [55]. Our viscosity value suggests that: i) viscosity measurements have a strong

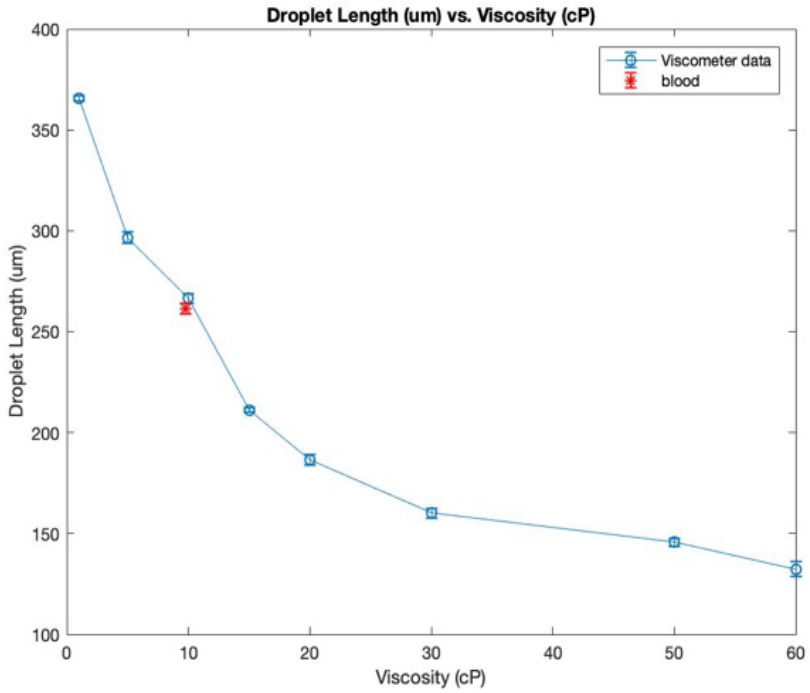

Figure 3.2.2 Blood viscosity measurements using microfluidic viscometer: The same graph from Figure 2.7.3c with an added data point from the blood experiments. The red star data point represents droplet length obtained from the blood sample at the same flow rate, 11psi(aqueous)-22psi(oil). Data from the blood experiments is in agreement with the data from the glycerol solutions. Error bars represent standard deviation for each data point.

temperature dependence, and the sample temperature was not close to the ideal (37°C). ii) Despite the presence of anticoagulants, the viscosity value was above the expected value

due to partial coagulation. Finally, we plotted droplet length as a function of inlet pressure ratio (AIP/OIP) for the human whole blood sample (Figure 3.2.3). As expected, we observed that, the droplet length increases with increasing AIP/OIP ratio where the OIP is kept constant. A linear fit as shown in Figure 3.2.3 can be used to determine the minimum possible droplet length that can be generated for a given OIP value. Overall, we demonstrated that our microfluidic viscometer can be used to determine the viscosity of human whole blood samples.

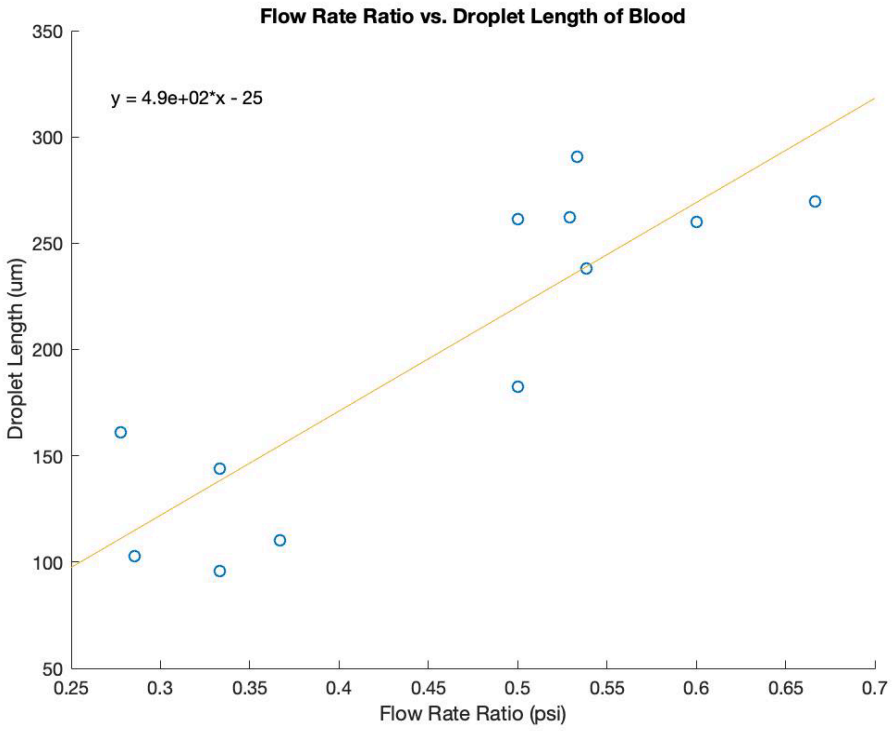

Figure 3.2.3 Droplet length of blood samples as a function of AIP/OIP: Droplet length increases as the aqueous inlet pressure increases at a constant oil inlet pressure. As a result, droplet length increases with the flow rate ratio.

Chapter IV

Conclusion and Future Work

4.1 Conclusion

With our results, we have demonstrated the application of droplet-based microfluidic viscometers towards continuous measurement of viscosities for diagnostic analysis. Our approach provides a simple and low-cost method to detect viscosity changes in biofluids. Our method offers additional advantages for biological applications where samples are difficult to obtain or costly, particularly when continuous monitoring is necessary. This droplet-based microfluidic viscometer can measure viscosity of Newtonian and non-Newtonian fluids, including biological fluids. The pressure-driven flow and small channel size make it an ideal device for monitoring blood viscosity in cardiovascular applications.

Our droplet-based viscometer provides a simple way to measure viscosity using a minute sample size. With a pressure or a vacuum source to drive fluids within the device, the viscometer could be applied along with other microfluidic processes such as droplet-based polymerization reactions to measure viscosity, improve uniformity performance of the products. The viscosity changes can be visualized and analyzed based on the length of the droplets or be measured in real-time with an on-chip sensor. This viscometer can be used to measure absolute viscosities at different shear rates or measuring viscosity changes

at a constant shear rate during a reaction leading to viscosity changes to monitor progression of biological reactions such as in blood coagulation.

4.2 Future Work

We demonstrated that our microfluidic device is capable of generating aqueous droplets with viscosities ranging from 1 to 60 cP into a carrier oil medium. We used our platform to measure viscosity of human whole blood samples. When conducting blood experiments, the blood sample was stored in vacutainers containing anticoagulants. To initiate clot formation, $CaCl_2$ was added to the blood sample prior to loading on the microfluidic viscometer. However, once the coagulant is added, the blood coagulation begins immediately. The time that it takes for the sample to travel the distance between the sample vial and the microfluidic junction where the droplets are formed, limits the accuracy of the viscosity measurement. Future versions of μVHA could facilitate on-chip activation of coagulation by automatic mixing of coagulation activators and enable multiplexing to concurrently run multiple versions of VHAs [2, 44].In the future, we would like to explore a device design that administers the coagulant on chip, thereby minimizing the risk for undesired clot formation and potential clogging of the device (Figure 4.2.1). This design comprises of two oil inlets, one inlet for blood, and one inlet for coagulant. In addition, the design will include serpentine channels to allow for efficient on-chip mixing of the blood and the coagulant prior to droplet generation. Our next step would be to explore whether the coagulant can be mixed on chip. Ultimately, generating droplets through all stages of clot formation would help generate clot firmness curves similar to those obtained by TEG and TEM.

In the future, our droplet-based microfluidic viscometer can be automated for point-of-care applications. Droplet parameters including droplet length and inter-droplet distance could be automatically measured and analyzed, and viscosities can be displayed in real-time by incorporating on-chip electrodes enabling capacitive sensing (6). This viscometer could also be expanded/adapted to measure viscosity of blood plasma, deformability of red blood cells and kinetics of blood coagulation. By expanding the applications of the viscometer, this device could benefit patients and healthcare professionals, including emergency physicians, hematologists, surgeons, blood banks, and military medics. However, for developing a lab-on-a-chip device capable of conducting all of these tests, integration of components such as droplet generation, separation of whole blood into blood cells and plasma, mixing of reagents with blood droplets to trigger blood coagulation, and cell deformability assays are needed.

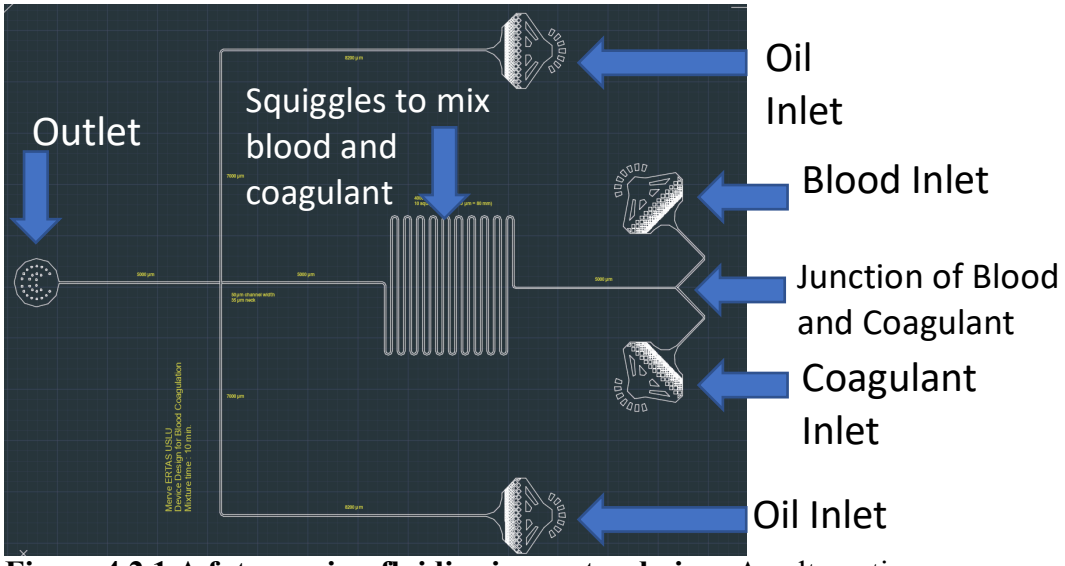

Figure 4.2.1 A future microfluidic viscometer design: An alternative device design for enabling on-chip mixing of coagulants for future experiments.

References

1. Li, Y., *Continous Microfluidic Viscometer for Biochemical and Diagnostic Analysis*, in *Biomedical Engineering*. 2017, University of Michigan.
2. Evans, A., et al., *Viscoelastic Hemostatic Assays - A Quest for Holy Grail of Coagulation Monitoring in Trauma Care.* Journal of Annals of Bioengineering, 2019. **1**: p. 61-64.
3. Thakur, M. and A.B. Ahmed, *A Review of Thromboelastography.* International Journal of Perioperative Ultrasound and Applied Technologies, 2012. **1**(1): p. 25-29.
4. Whitesides, G.M., *The origins and the future of microfluidics.* Nature, 2006. **442**(7101): p. 368-373.
5. Rivet, C., et al., *Microfluidics for medical diagnostics and biosensors.* Chemical Engineering Science, 2011. **66**(7): p. 1490-1507.
6. Olanrewaju, A., et al., *Capillary microfluidics in microchannels: from microfluidic networks to capillaric circuits.* Lab on a Chip, 2018. **18**(16): p. 2323-2347.
7. Teh, S.-Y., et al., *Droplet microfluidics.* Lab on a Chip, 2008. **8**(2): p. 198-220.
8. Sachdeva, S., R.W. Davis, and A.K. Saha, *Microfluidic Point-of-Care Testing: Commercial Landscape and Future Directions.* Frontiers in Bioengineering and Biotechnology, 2021. **8**(1537).
9. Palta, S., R. Saroa, and A. Palta, *Overview of the coagulation system.* Indian journal of anaesthesia, 2014. **58**(5): p. 515-523.

10. Goodman, D.M., A.E. Burke, and E.H. Livingston, *Bleeding Disorders.* JAMA, 2012. **308**(14): p. 1492-1492.

11. Gonzalez, E., et al., *Goal-directed Hemostatic Resuscitation of Trauma-induced Coagulopathy: A Pragmatic Randomized Clinical Trial Comparing a Viscoelastic Assay to Conventional Coagulation Assays.* Annals of surgery, 2016. **263**(6): p. 1051-1059.

12. Hartmann, J., M. Murphy, and J.D. Dias, *Viscoelastic Hemostatic Assays: Moving from the Laboratory to the Site of Care-A Review of Established and Emerging Technologies.* Diagnostics (Basel, Switzerland), 2020. **10**(2): p. 118.

13. Tur Martínez, J., et al., *Comparison Between Thromboelastography and Conventional Coagulation Test: Should We Abandon Conventional Coagulation Tests in Polytrauma Patients?* Cirugía Española (English Edition), 2018. **96**(7): p. 443-449.

14. Whiting, P., et al., *Viscoelastic point-of-care testing to assist with the diagnosis, management and monitoring of haemostasis: a systematic review and cost-effectiveness analysis.* Health Technol Assess, 2015. **19**(58).

15. Grover, S.P. and N. Mackman, *Intrinsic Pathway of Coagulation and Thrombosis.* Arteriosclerosis, Thrombosis, and Vascular Biology, 2019. **39**(3): p. 331-338.

16. Winter, W.E., S.D. Flax, and N.S. Harris, *Coagulation Testing in the Core Laboratory.* Laboratory Medicine, 2017. **48**(4): p. 295-313.

17. Silver, B.J., *Prolongation of Both PT and aPTT*, in *The Coagulation Consult: A Case-Based Guide*, A. Lichtin and J. Bartholomew, Editors. 2014, Springer New York: New York, NY. p. 71-85.

18. Capoor, M.N., et al., *Prothrombin Time and Activated Partial Thromboplastin Time Testing: A Comparative Effectiveness Study in a Million-Patient Sample.* PloS one, 2015. **10**(8): p. e0133317-e0133317.

19. Ebner, M., et al., *Limitations of Specific Coagulation Tests for Direct Oral Anticoagulants: A Critical Analysis.* Journal of the American Heart Association, 2018. **7**(19): p. e009807.

20. Ganter, M.T. and C.K. Hofer, *Coagulation Monitoring: Current Techniques and Clinical Use of Viscoelastic Point-of-Care Coagulation Devices.* Anesthesia & Analgesia, 2008. **106**(5).

21. McMichael, M.A. and S.A. Smith, *Viscoelastic coagulation testing: technology, applications, and limitations.* Veterinary Clinical Pathology, 2011. **40**(2): p. 140-153.

22. Serraino, G.F. and G.J. Murphy, *Routine use of viscoelastic blood tests for diagnosis and treatment of coagulopathic bleeding in cardiac surgery: updated systematic review and meta-analysis.* BJA: British Journal of Anaesthesia, 2017. **118**(6): p. 823-833.

23. Johansson, P.I., et al., *Thrombelastography and tromboelastometry in assessing coagulopathy in trauma.* Scandinavian Journal of Trauma, Resuscitation and Emergency Medicine, 2009. **17**(1): p. 45.

24. Ko, R.H., L. Ji, and G. Young, *A novel approach for detecting hypercoagulability utilizing thromboelastography.* Thrombosis Research, 2013. **131**(4): p. 352-356.

25. Park, M.S., et al., *Thromboelastography as a better indicator of hypercoagulable state after injury than prothrombin time or activated partial thromboplastin time.* The Journal of trauma, 2009. **67**(2): p. 266-276.

26. Sahli, S.D., et al., *Point-of-Care Diagnostics in Coagulation Management.* Sensors (Basel, Switzerland), 2020. **20**(15): p. 4254.

27. Shen, L., S. Tabaie, and N. Ivascu, *Viscoelastic testing inside and beyond the operating room.* Journal of thoracic disease, 2017. **9**(Suppl 4): p. S299-S308.

28. Thachil, J., *Dispelling myths about coagulation abnormalities in internal medicine.* Clinical medicine (London, England), 2014. **14**(3): p. 239-244.

29. Brazzel, C., *Thromboelastography-Guided Transfusion Therapy in the Trauma Patient.* American Association of Nurse Anesthesists Journal, 2013. **81**(2): p. 127-132.

30. Johansson, P.I., *Coagulation monitoring of the bleeding traumatized patient.* Curr Opin Anaesthesiol, 2012. **25**(2): p. 235-41.

31. Benes, J., J. Zatloukal, and J. Kletecka, *Viscoelastic Methods of Blood Clotting Assessment – A Multidisciplinary Review.* Frontiers in Medicine, 2015. **2**: p. 62.

32. Jackson, G.N.B., K.J. Ashpole, and S.M. Yentis, *The TEG® vs the ROTEM® thromboelastography/thromboelastometry systems.* Anaesthesia, 2009. **64**(2): p. 212-215.

33. Levrat, A., et al., *Evaluation of rotation thrombelastography for the diagnosis of hyperfibrinolysis in trauma patients.* British Journal of Anaesthesia, 2008. **100**(6): p. 792-797.

34. Bolliger, D., M.D. Seeberger, and K.A. Tanaka, *Principles and Practice of Thromboelastography in Clinical Coagulation Management and Transfusion Practice.* Transfusion Medicine Reviews, 2012. **26**(1): p. 1-13.

35. Fleming, K., et al., *TEG-Directed Transfusion in Complex Cardiac Surgery: Impact on Blood Product Usage.* The journal of extra-corporeal technology, 2017. **49**(4): p. 283-290.

36. Wang, S.C., et al., *Thromboelastography-Guided Transfusion Decreases Intraoperative Blood Transfusion During Orthotopic Liver Transplantation: Randomized Clinical Trial.* Transplantation Proceedings, 2010. **42**(7): p. 2590-2593.

37. Kang, Y.G., et al., *Intraoperative Changes in Blood Coagulation and Thrombelastographic Monitoring in Liver Transplantation.* Anesthesia & Analgesia, 1985. **64**(9).

38. Karkouti, K., et al., *Point-of-Care Hemostatic Testing in Cardiac Surgery.* Circulation, 2016. **134**(16): p. 1152-1162.

39. Cohen, T., T. Haas, and M.M. Cushing, *The strengths and weaknesses of viscoelastic testing compared to traditional coagulation testing.* Transfusion, 2020. **60**(S6): p. S21-S28.

40. Yeung, M.C., et al., *Use of viscoelastic haemostatic assay in emergency and elective surgery.* Hong Kong Med J, 2015. **21**(1): p. 45-51.

41. Hans, G.A. and M.W. Besser, *The place of viscoelastic testing in clinical practice.* British Journal of Haematology, 2016. **173**(1): p. 37-48.

42. Hartert, H., *Blutgerinnungsstudien mit der Thrombelastographie, einem neuen Untersuchungsverfahren.* Klinische Wochenschrift, 1948. **26**(37): p. 577-583.

43. Li, Y., K.R. Ward, and M.A. Burns, *Viscosity Measurements Using Microfluidic Droplet Length.* Analytical Chemistry, 2017. **89**(7): p. 3996-4006.

44. Mena, S.E., et al., *A droplet-based microfluidic viscometer for the measurement of blood coagulation.* Biomicrofluidics, 2020. **14**(1): p. 014109.

45. Choi, K., et al., *Digital Microfluidics.* Annual Review of Analytical Chemistry, 2012. **5**(1): p. 413-440.

46. Guo, M.T., et al., *Droplet microfluidics for high-throughput biological assays.* Lab on a Chip, 2012. **12**(12): p. 2146-2155.

47. DeLaMarre, M.F., A. Keyzer, and S.A. Shippy, *Development of a Simple Droplet-Based Microfluidic Capillary Viscometer for Low-Viscosity Newtonian Fluids.* Analytical Chemistry, 2015. **87**(9): p. 4649-4657.

48. Srivastava, A. and A. Kelleher, *Point-of-care coagulation testing.* Continuing Education in Anaesthesia Critical Care & Pain, 2013. **13**(1): p. 12-16.

49. Leeper, C.M. and B.A. Gaines, *Viscoelastic hemostatic assays in the management of the pediatric trauma patient.* Seminars in Pediatric Surgery, 2017. **26**(1): p. 8-13.

50. Gupta, S., W.S. Wang, and S.A. Vanapalli, *Microfluidic viscometers for shear rheology of complex fluids and biofluids.* Biomicrofluidics, 2016. **10**(4): p. 043402.

51. Judith, R.M., et al., *Micro-elastometry on whole blood clots using actuated surface-attached posts (ASAPs).* Lab on a Chip, 2015. **15**(5): p. 1385-1393.

52. Jang, I., K.E. Berg, and C.S. Henry, *Viscosity measurements utilizing a fast-flow microfluidic paper-based device.* Sensors and Actuators B: Chemical, 2020. **319**: p. 128240.

53. Saito, M., et al., *Field-deployable rapid multiple biosensing system for detection of chemical and biological warfare agents.* Microsystems & Nanoengineering, 2018. **4**(1): p. 17083.

54. Xia, Y. and G.M. Whitesides, *Soft Lithography.* Angewandte Chemie International Edition, 1998. **37**(5): p. 550-575.

55. Ranucci, M., et al., *Blood viscosity during coagulation at different shear rates.* Physiological reports, 2014. **2**(7): p. e12065.

56. Moore, E.E., et al., *Trauma-induced coagulopathy.* Nature Reviews Disease Primers, 2021. **7**(1): p. 30.

57. Martini, W.Z., *Coagulation complications following trauma.* Military Medical Research, 2016. **3**: p. 35-35.